Neutron-Proton Forward-Angle Elastic Cross Sections at 790 MeV

R. Carlini,[a] B. Dieterle, J. Donahue,[a] C. Leavitt, T. Rupp,[b] W. Thomas,[c] and D. Wolfe
Department of Physics and Astronomy, University of New Mexico, Albuquerque, New Mexico 87131

and

L. B. Auerbach, V. L. Highland, K. F. Johnson,[d] and W. K. McFarlane
Temple University, Philadelphia, Pennsylvania 19122

and

J. Pratt and R. Bentley
Los Alamos Scientific Laboratory, Los Alamos, New Mexico 87545
(Received 9 June 1978)

High-statistics measurements of the absolute differential cross section for n-p scattering have been made over neutron c.m.-system scattering angles $9.5° < \theta^* < 64.5°$. The statistical error is 1.7 to 3.3% for 2°-wide angular bins, and the systematic error is 2.7 to 3.3%. The cross section is fitted by $d\sigma/d\Omega^* = A \exp(bt)$, with $A = 10.27 \pm 0.36$ mb/sr, $b = 5.00 \pm 0.05$, and $0.01 < -t < 0.39$ $(\mathrm{GeV}/c)^2$. For the ratio of the real to the imaginary part of the forward-scattering amplitude we obtained $\alpha_n \geq -0.43 \pm 0.04$, consistent with other less precise determinations of α_n.

The data we present here are the first results of a series of high-precision measurements of the forward-angle neutron-proton differential cross section at the Clinton P. Anderson Meson Physics Facility (LAMPF). These are the only measurements of this kind above pion production threshold that have errors of only a few percent and extend to four-momentum transfers as small as $-t \sim 0.01$. They should have immediate use in the interpretation of proton-nucleus scattering data at medium energies, since knowledge of the p-n interaction (and the p-p interaction) is essential if the proton is to be used as a probe of the nucleus. Accurate ($\lesssim 2\%$) forward n-p elastic scattering cross sections have been found to be important[1] to phase-shift solutions below 500 MeV. We expect that this will also be the case at 800 MeV and that numerous accurate measurements such as these will be necessary to determine completely the fundamental neutron-proton scattering amplitudes. Backward-angle n-p measurements[2] at 800 MeV have been made which complement these.

Below 400 MeV, phase-shift solutions have been obtained and one-boson–exchange models give reasonable fits to the data. This is not so above 400 MeV where there are fewer accurate data. The problem is complicated by large inelastic effects which affect elastic scattering through unitarity. Phase-shift solutions for n-p elastic scattering do not exist here and one-boson–exchange models are inadequate because they violate unitarity. In spite of this, we have some qualitative understanding in this energy region. The pion production cross section rises from ~1 mb at 400 MeV to ~10 mb at 800 MeV. This is accompanied by a shift of the elastic angular distribution from mainly backward to mainly forward. The increase in forward scattering is due to increased diffraction scattering around a proton target that appears blacker as the inelastic channels open up with increasing energy. At the relatively low energy of 790 MeV, we observe that the elastic cross section has the exponential dependence on t that is characteristic of diffraction scattering.

The experimental technique used to detect forward scattering was neutron time of flight (TOF). This was possible because of the existence of a pulsed (40- or 80-ns period), almost monoenergetic neutron beam at LAMPF (see Fig. 1). Elastically scattered 790-MeV neutrons arrived at the neutron detector at a unique time relative to the primary beam burst from the accelerator. This allowed elastic events to be identified without observation of the recoil proton and without the accompanying restrictions on momentum transfer caused when recoil protons stop inside the target flask. The fact that we were able to select elastic events in this way had two very beneficial consequences: (1) Neutron-proton scattering events could be observed at very small angles, and (2) absolute cross sections could be obtained without knowledge of the beam flux or the detector efficiency, as shown below.

An 800-MeV proton beam of intensity $\simeq \frac{1}{2}$ μA with 40-ns structure incident upon a 10.6-cm liquid-deuterium (LD_2) target produced the neu-

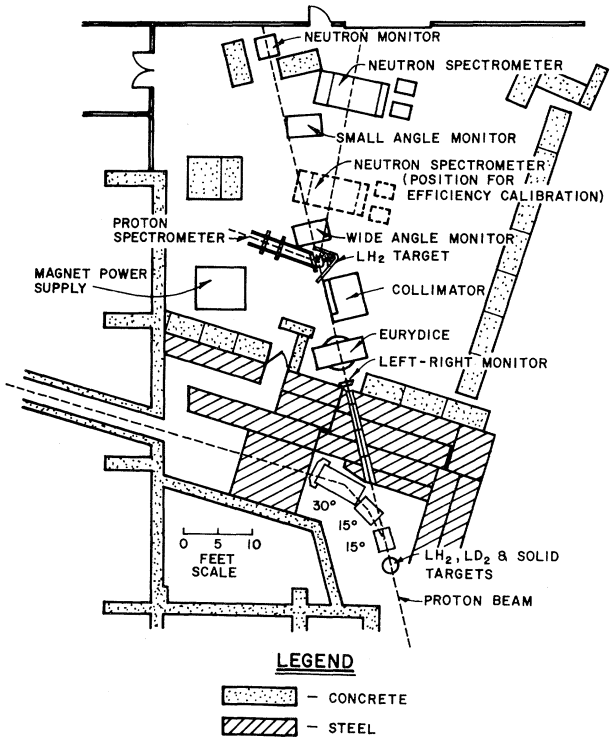

FIG. 1. Neutron beam and apparatus in Area B at LAMPF.

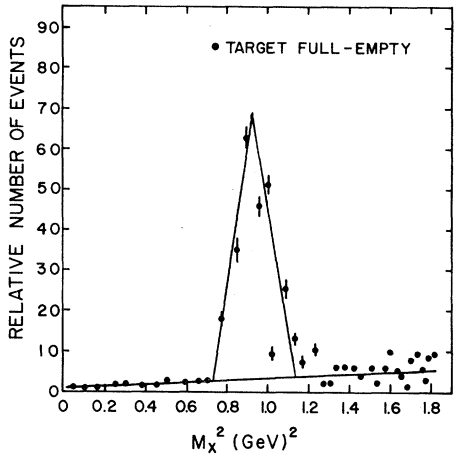

FIG. 2. Spectrum of the square of the recoil missing mass at 4° lab angle. The lines are to guide the eye along the background and the peak for elastic proton recoils.

tron beam. The spectrum at 0° consisted of a peak $\lesssim 15$ MeV wide and a broad low-energy tail, each with about 150 000 neutrons/sec. A 1-in.-diam, steel collimator directed the beam onto a $2\frac{1}{2}$-in.-diam.$\times$12-in.-long liquid-hydrogen (LH_2) target. A second collimator was located on the scattered-neutron side of the beam to prevent particles produced in the first collimator from reaching the neutron detector (N). The detector consisted of a veto counter (V) to eliminate charged particles, a carbon slab 4 in. thick$\times$12 in. $\times$24 in. to convert neutrons into charged particles, four multiwire-proportional-counter ($W_1 - W_4$) to project charged tracks back to the converter, and a TOF counter (N_A) to measure the neutron conversion time relative to the rf chopper time. A recoil-proton telescope was located at the angle conjugate to the neutron scattering angle. If a proton had sufficient energy to exit from the LH_2, its orbit was determined using three helical proportional counters. Each of these encoded an X-Y coordinate. Scintillation counters in the proton arm were used to measure the time of the recoil track. Helium bags in the beam reduced the neutron scattering from gas in the beam line.

A trigger consisted of a count in the neutron detector which had the logic $N \equiv \overline{V} \cdot N_A \cdot (W_1 \cdot W_2 \cdot W_3 \cdot W_4)_{3/4}$ (≥ 3 of the four W counters fired). An on-line computer system was used to sort and write data on magnetic tape and monitor the experiment.

Elastically scattered 790-MeV neutrons appeared as a peak in the neutron TOF spectrum, where the N_A counter time minus the rf chopper time defines the TOF. Clean separation of these events is shown in Fig. 2. Most of the nonelastic events were removed by keeping only events within 1.2 ns from the center of the neutron peak. An additional cut rejected events outside a fiducial region 20 cm$\times$56 cm centered on the carbon converter. A correction to the number of elastic neutrons was made to account for γ-ray contamination. Neutral-pion production by 500-MeV neutrons made γ rays which arrived at the neutron detector with the same total TOF from the LD_2 as 790-MeV elastically scattered beam neutrons. This (6 to 20%) contamination was measured and subtracted, causing $< 1.5\%$ error in our cross sections. The relative neutron flux was monitored by counters upstream (left-right monitor) and downstream (neutron monitor) of the LH_2 flask. The beam flux through the flask was monitored using charged-particle counter telescopes at 10° and 45°. These monitors all tracked to better than 1%.

Absolute differential cross sections depend on the ratio of the rates for the neutron detector in

the beam (R_{in}) and out of the beam (R_{out}):

$$\frac{R_{out}}{R_{in}} = \frac{\bar{\epsilon} R_B \rho t \, d\sigma/d\Omega}{\epsilon_c R_B} = \frac{\bar{\epsilon}}{\epsilon_c} \rho t \frac{d\sigma}{d\Omega},$$

where R_B is the beam flux per monitor counts, $\rho t = (1.227 \pm 0.012) \times 10^{24}$ protons/cm^2, R_{out} and R_{in} are the count rates per relative monitor count for the detector at θ^{lab} and 0°, respectively, ϵ_c is the efficiency at the center of the neutron spectrometer, and $\bar{\epsilon}$ is the efficiency for neutrons averaged over the appropriate angular bin in the laboratory.

The ratio $\epsilon_c/\bar{\epsilon}$ is equal to 1 if the detector has no energy dependence and a flat response across its face. The true spatial response varied less than 25% when the beam was moved to different points within the fiducial region (20 cm×56 cm) of the converter. This mapping determined $\epsilon_c/\bar{\epsilon}$ to about 1%. $\bar{\epsilon}$ was found to have an energy dependence that was linear and had a slope of (9.6 ± 0.6)%/(100 MeV). This gives the largest error on $\epsilon_c/\bar{\epsilon}$ of 1.5% (at θ^{max}). The slope was measured in a special geometry (see Fig. 1) using the proton arm as the event trigger. The fraction of neutrons converting at the predicted location in the neutron detector equals the efficiency.

Other errors and corrections such as ortho-hydrogen-parahydrogen fractions, target density, error due to TOF cuts, floor scattering, monitor dead time, charged particles misidentified as neutrons, double scattering, fiducial area, etc., are estimated to each be < 1%. The (systematic, random) error is estimated to be (2.7% to 3.3%, 2% to 4%), depending on angle, for 1°-wide bins in the laboratory.

The differential cross sections were measured at nine different detector laboratory angles covering 3.5° to 29.5°. The carbon converter was divided into four bins 1° wide in the laboratory (about 2° wide in the c.m. system). These bins overlapped with neighboring laboratory-angle detector settings. The exponential form is fitted with a χ^2 of 55 for 34 degrees of freedom when only statistical errors are included. Inclusion of systematic errors gives

$$d\sigma/d\Omega^* = (10.27 \pm 0.36) \exp[(5.00 \pm 0.05)t] \text{ mb/sr},$$

where the intercept error is mainly due to systematic errors and the slope error is mainly due to statistical errors. This plot is shown in Fig.

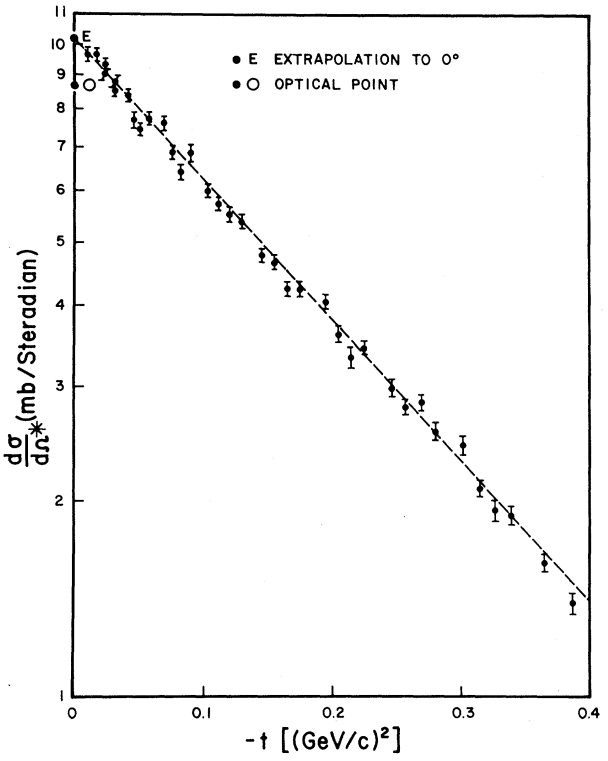

FIG. 3. Differential cross section and exponential fits (see text).

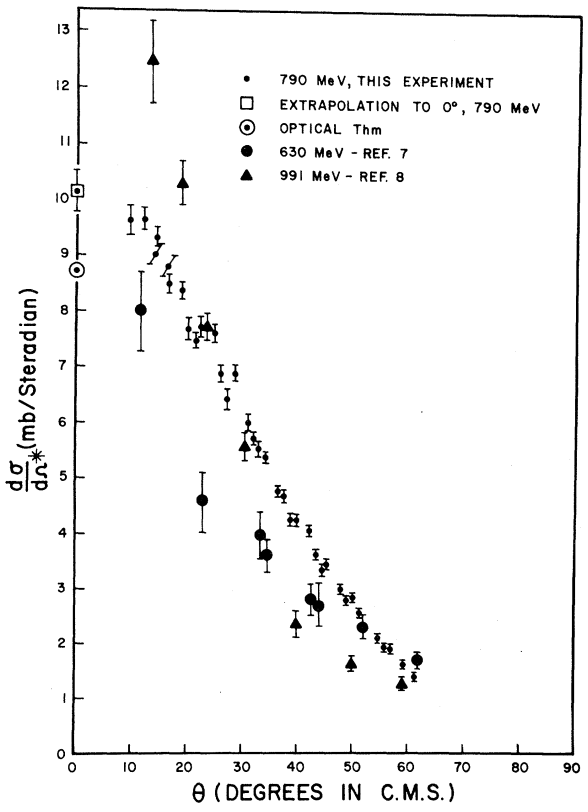

FIG. 4. Differential cross section compared to other experiments.

3. At high energies b is about 8, because of the greater absorption.

Figure 4 shows our measurements plotted with data at the two nearest energies,[3,4] for qualitative comparison. The optical theorem gives the value of the imaginary part of the square of the forward-scattering amplitude to be 8.68 ± 0.05 mb/sr.[5] Using a simple exponential model for extrapolation[6] we have

$$d\sigma/d\Omega^* = |f_{\mathrm{opt}}|^2(1+\alpha_n^2+\beta_n^2)e^{bt},$$

where $f_{\mathrm{opt}} = k\sigma_{\mathrm{tot}}/4\pi$ is the mean value of the imaginary part of the spin-dependent amplitudes, α_n is the rms value of the real part of the spin-dependent amplitudes, and β_n is the rms deviation of the imaginary part of the amplitudes from f_{opt}. From this we obtain

$$(\alpha_n^2+\beta_n^2)^{1/2} = 0.41 \pm 0.04, \quad \alpha_n \geq -0.43 \pm 0.04,$$

where we have assumed that the sign is negative as determined by other methods.[6,7]

Using a small-angle p-d scattering technique, Dutton and van der Raay[8] obtained α_n and β_n at four-momenta from 1.29 to 1.69 GeV/c. We have averaged their results to obtain $(\alpha_n^2+\beta_n^2)^{1/2} = 0.56 \pm 0.18$, $\alpha_n = -0.48 \pm 0.16$, and $\beta_n = 0.26 \pm 0.26$. Using dispersion techniques Bugg and Carter[7] obtained $\alpha_n = -0.32 \pm 0.20$. Our result is consistent with these values, but because of the large error bars on α_n an improved value of β_n cannot be obtained. Since backward-angle n-p scattering[9] shows effects due to π^+ exchange for $-u < 0.01$ (GeV/c)^2 the possibility exists[2] that π° exchange at $-t < 0.01$ (GeV/c)^2 would change the slope and intercept from our values. This effect has been ignored in past publications and will be the subject of further investigation by us.

We would like to thank C. Gregory, J. Valentine, J. Hontas, J. Sanchez, H. Balsham, N. Colella, K. Dhingra, and the LAMPF staff, especially R. Werbeck and D. West, for their help on various aspects of this experiment. This work was supported by the U. S. Department of Energy.

[a]Present address: Los Alamos Scientific Laboratory, Los Alamos, N. M. 87544.
[b]Present address: EG&G, Albuquerque, N. M. 87106.
[c]Present address: Science Applications, Inc., Albuquerque, N. M.
[d]Present address: Schweizerisches Institut für Nuklearforschung, Zürich, Switzerland.

[1]D. V. Bugg, TRIUMF Report No. TRI-75-5, 1975 (unpublished).
[2]B. Dieterle, in *Nucleon-Nucleon Interactions—1977*, AIP Conference Proceedings No. 41, edited by H. Fearing, D. Measday, and A. Strathdee (American Institute of Physics, New York, 1978).
[3]N. S. Amaglobelli and Yu M. Kazarinov, Zh. Eksp. Teor. Fiz. 37, 1587 (1959) [Sov. Phys. 10, 1125 (1960)].
[4]R. A. Murray *et al.*, Nuovo Cimento 49, 261 (1967).
[5]T. J. Devlin *et al.*, Phys. Rev. D 8, 136 (1973).
[6]L. M. C. Dutton and H. B. van der Raay, Phys. Lett. 26B, 697 (1968).
[7]D. V. Bugg and A. A. Carter, Phys. Lett. 20, 203 (1964).
[8]L. M. C. Dutton and H. B. van der Raay, Phys. Rev. Lett. 21, 1416 (1968).
[9]M. L. Evans *et al.*, Phys. Rev. Lett. 36, 497 (1976).

Vacuum Polarization at Long Distances and the Heavy-Quark–Antiquark Potential

Enrico C. Poggio and Howard J. Schnitzer
Department of Physics, Brandeis University, Waltham, Massachusetts 02154
(Received 20 July 1978)

Vacuum polarization at long distances for confined heavy-quark–antiquark ($Q\bar{Q}$) pairs is considered. The vacuum-polarization–corrected static potential is shown to have a radial dependence which should allow interpolation between charmonium, upsilon states, and other heavy $Q\bar{Q}$ systems. It is argued that the static, confining potential cannot grow faster than a linear potential at large distances, within the framework of this analysis.

Heavy-quark–antiquark ($Q\bar{Q}$) spectroscopy is generally regarded as being well described phenomenologically by a nonrelativistic potential model, with a static, quark-confining potential.[1] Along with the model, one has the understanding that there are (at least) two importnat regions of coordinate space, roughly described by $r \lesssim (\alpha_s m)^{-1} \simeq a_0$, where quantum-chromodynamic (QCD) per-

